doi.org/10.1002/batt.202000088

A New Technique for In Situ Determination of the Active Surface Area Changes of Li–Ion Battery Electrodes

Maciej Ratynski,[a] Bartosz Hamankiewicz,*[a] Dominika A. Buchberger,[a] Maciej Boczar,[a] Michał Krajewski,[a] and Andrzej Czerwinski[a]

Li-ion batteries have been of a great interest for over three decades. A geometric electrode surface area is generally used for Li-ion electrochemical parameters calculations. Since the real electrode is a complex system composed of the thick porous structure, the contact surface area between the active mass and electrolyte is far larger than geometrical. This approximation leads to a large deviation of obtained results, especially within different laboratories and for volume and surface changing materials, e.g., silicon. The article presents a new method of in situ analysis of active surface area variations applicable for Li-ion electrodes. The method relies on the electrochemical impedance spectroscopy measurement (EIS) performed at an arbitrarily chosen state of charge during superimposed DC current flow. The correlation between a local ion concentration with a charge transfer resistance allows to evaluate the differences of the active surface area. The presented method is not affected by the SEI layer presence, the material composition, nor the lithiation mechanism. Due to limited EIS frequency range the presented method can be performed with a relatively short time. Our new in situ surface area determination can greatly improve the accuracy of the electrochemical parameters evaluation and enable the proper result analysis. We believe that our method can become a standard procedure implemented in every research focusing on the electrochemical parameter determination of the volume changing active materials.

1. Introduction

Lithium-ion batteries became exceptionally important for the energy storage industry over the last three decades. Recently new types of conversion materials are intensively investigated as a possible negative electrode replacement for the commonly used graphite. The application of tin,[1] germanium,[2] aluminum[3] and silicon[4] is the main research direction. In contrast with graphite, all these materials present a very high specific capacity, as well as a high volume change during a lithium uptake. The high specific capacity justifies the vast number of the research focusing on the new, alloy-type materials utilization. Silicon has the highest specific capacity of all known alloy-type anode materials and it is close to 3570–4200 mAh/g (~1860 mAh/g when lithium mass is included).[5,6] It also presents the lowest specific volume change per charge unit ~0.08% g/mAh, even though, the total volume change may exceed 290% during the full silicon lithiation. This results in fast mechanical degradation of the electrode macro-structure, as well as individual grain pulverization and cracking.[7–9] Several theoretical models were invented for the lithiation induced stress estimation and a better understanding of silicon electrode failure mechanisms.[10–14] These models are based on several simplifications such as the isolated particle approximation or matrix properties averaging. As a result, those models give detailed insight into the stress evolution inside a silicon particle, however, provides a very limited information about particles surface changes or the overall electrode morphology changes.

The electrochemically active surface area (ECSA) of the electrode is the primary electrochemical factor affecting all electrochemical measurements. Each of the experiments involves the measurement of the voltage vs. current relation. In the voltage-controlled measurement, the total current is directly dependent on the electrode surface and the current density. Then the ECSA affects all estimated electrochemical parameters of the system. The ECSA or real surface area (RSA) is always larger than geometrical due to surface roughness or multilayer nanoparticle stacking.[15–18] The difference may exceed 3 orders of magnitude leading to essential inaccuracy of determined system parameters.

The investigation of ECSA has been widely reported for noble metals (Pt, Au) and their alloys or glassy carbon electrodes.[15,17] For noble metals electrodes a hydrogen adsorption/desorption charge is used since it is proportional to the number of active sites and RSA. The method is applicable only for the limited materials that do not absorb the hydrogen. Even for these relatively simple systems, the empirically determined coverage factor and the specific surface charge, as well as the edge effect simplification lead to the limited method accuracy.[15] Another good method of the ECSA estimation is the double layer (DL) formation charge measurement during cyclic voltammetry (CV) experiment. This method provides accurate results, but is limited to the voltage range

[a] Dr. M. Ratynski, Dr. B. Hamankiewicz, Dr. D. A. Buchberger, M. Boczar, Dr. M. Krajewski, Prof. Dr. A. Czerwinski
Faculty of Chemistry
University of Warsaw
L. Pasteura 1, 02-093 Warsaw, Poland
E-mail: bhamankiewicz@chem.uw.edu.pl

Supporting information for this article is available on the WWW under https://doi.org/10.1002/batt.202000088

outside any faradaic reaction and requires the knowledge of the empirically determined specific surface charge value. The method utilization is also limited to the systems, in which small ions (especially hydrogen) are adsorbed. Larger ions will present much smaller coverage factor due to the steric repulsion leading to a decrease of this method accuracy. The DL capacity measurement use for ECSA determination in Li-ion system is very limited or even impossible. The faradaic lithiation reaction will affect the obtained data leading to highly inaccurate results. On the other hand, performing the experiment outside the lithiation/delithiation potential window does not provide any information about ECSA variations during the reaction progress. Moreover, for the majority of Li-ion battery materials it is impossible to reach the potential region outside Faradaic reactions and in some cases such an attempt may lead to a permanent electrode degradation due to oxidation, crystal structure collapse and/or undesired SEI formation. Measuring the absolute DL capacity in the lithiation potential window by the electrochemical impedance spectroscopy (EIS) experiment is also limited due to a slow diffusion of solvated Li^+ cations and large anions. This leads to the slow DL charging resulting in the DL formation time greater than the charge transfer (CT) time constant. Consequently, the faradaic reaction affects the experiment hindering the capacity processes. An implementation of other methods used for noble metal electrodes such as CO adsorption and metal underpotential deposition[19] into Li-ion system are likewise impossible.

All the above discussed methods are designed for relatively flat and metallic electrode surface examination. For porous powders the gas adsorption or spectroscopic methods are generally used for surface area determination. One of the most often used technique is a gas adsorption measurement. In this method, the amount of adsorbed gas (typically nitrogen) is referred to the surface area of the measured powder. Various analytical methods has been proposed to determine the relationship between the adsorbed gas volume and the adsorbate surface area. The most common is known as Brunauer-Emmet-Teller isotherm (BET). The adsorption profile provide additional information about pores sizes and distribution.[20] The BET technique is widely used in the Li-ion field for a pristine powder surface area evaluation.[21–23] Generally, the higher the specific area of the powder, the higher the electrode ECSA and specific power are. This effect is mostly due to a shorter ion diffusion path inside grains[24,25] or a high double layer charge.[26] Unfortunately, the BET analysis has limited capabilities in evaluation of the electrode active surface area. The technique requires powder substrate of high surface – typically $>0.5\ m^2/g$. The electrode mass is typically applied on the metallic foil and its real surface to geometric area ratio is much lower, leading to decrease in measurement accuracy. Additionally, the powder specific area does not correspond directly with the electrode ECSA. The ECSA can be limited by thick SEI layer, pore closure after calendering and mutual blockage of an electrolyte access to the particles surface (Figure 1). This result in a very limited application of BET for the ECSA analysis.

Several additional methods of powder surface analysis have been also reported. The XRD technique allows for very precise measurements of the crystallites.[27,28] Unfortunately, the method is limited to the crystalline materials, and is not capable of multi-size grain surface area evaluation. The mercury porosimetry is often use for pore distribution analysis.[29] The obtained results are related to the pore volume and distribution rather than the sample surface. The method application to the Li-ion electrodes is also limited due to the ex situ procedure application. The nano-tomography (CT) imaging of the internal Li-ion electrode structure results in high-resolution 3D images and the possible average grain volume and surface analysis.[30] The CT slice thickness in a state of art experiments was close to 700 nm. The grain size of many of the Li-ion materials are below this size.[21] This excludes the nano-CT use for the ECSA evaluation.

In case of Li-ion battery materials, the specific volume change is more often determined instead of grain surface area changes. The volume change of some materials can be easily revealed by XRD measurement through unit cell parameters

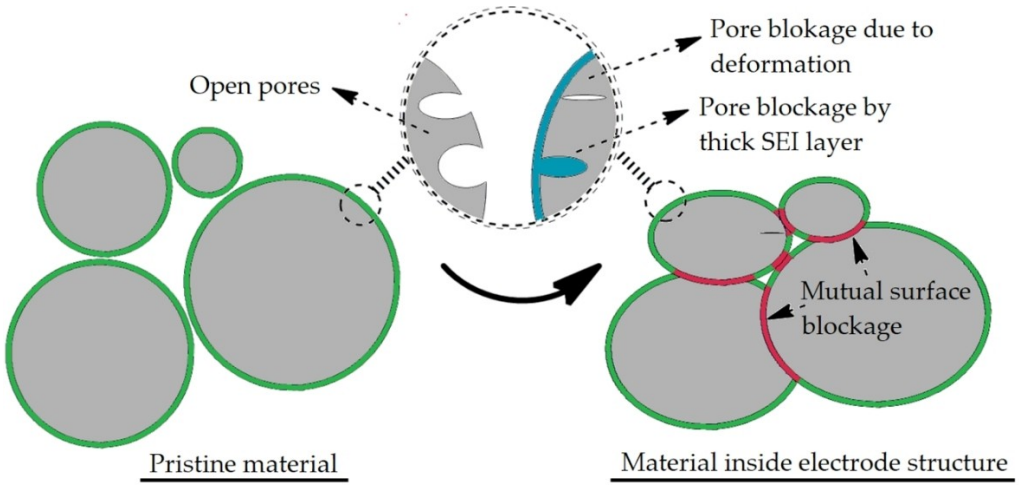

Figure 1. Schematic representation of active surface area difference between pristine powder and electrode material.

changes during lithiation.[31–33] Typical volume changes of layered cathode materials are not greater than 7–8%. The overall volume change of the material can be determined indirectly by open circuit voltage (OCV) measurement during isochoric conditions. The OCV is related to pressure applied into the active material grains (independently on the internal or external origin of pressure).[8,34] During the material expansion or shrinking the internal pressure will rise leading to changes in the measured potential. The formed pressure can also be directly measured with a proper equipment, when the material lithiation is continuously taking place .[31] The volume change of the material cannot be easily used to obtain the ECSA variation since the electrode often contains a blend of several micro-porous compounds as well as general macro-porous structure.

All presented methods have some kind of limitations. Most of them can only be used ex situ, which may affect the Li-ion electrode structure and ECSA changes as a consequence of a disassemble process. In case of Li-ion electrode, due to its high reactivity against air and water, may even lead to irreversible sample destruction.

As presented in Figure 1 the geometric and electroactive surface area of the Li-ion electrode can differ. The theoretical electrode active surface can be roughly estimated by Equation (1):[35]

$$S = \frac{V_{electrode} * (1-\varepsilon) * (1-N)}{V_{grain}} * (4\pi r^2) \quad (1)$$

where: $V_{electrode}$ is the active layer volume calculated from diameter and thickness coating, V_{grain} is the average grain volume from BET analysis, ε is the porosity, and N is the the relative volume fraction of inactive material (binder, conductive carbon etc.). The presented equation neglects the effect of calendering, SEI formation, material plastic deformation, volume change during lithiation and assumes spherical shape of all particles. All these simplifications lead to a large deviation of the estimated value.

During lithiation of the electrodes composed of volume expanding/depleting materials, the ECSA is dramatically changing, which results in the increased inaccuracy of the determined electrochemical parameters. For example, the lithium apparent diffusion coefficient in the silicon structure during lithiation differs from 10^{-14} to 10^{-10} cm^2/s depending on the measurement procedure. Even for the same procedure the value can change up to 100 times during silicon lithiation with no reasonable explanation.[36] Similar findings were published by other researchers, who observed lithium diffusion coefficient increase during silicon lithiation[37,38] or prolonged cycling.[39] The determined value of other electrochemical parameters, such as charge transfer resistance or SEI layer resistance, might also be affected by ECSA changes.[40] One of the most plausible explanation of the observed changes is the ECSA variation related to the silicon volume change during lithiation. Neglecting of ECSA changes during calculations may lead to faulty conclusions about the mechanism of degradation, electrochemical parameters changes or matrix stability issues. The knowledge about ECSA changes creates the correction factor that greatly maximize the results accuracy and increase the knowledge about electrode parameters changes during operation in the Li-ion battery.

Most of the Li-ion active materials are covered by some kind of interface layer. For the negative electrode materials working below ~0.7 V vs Li, the SEI layer formation is expected. For the layered metal oxides cathodes (e.g., NMC) the formation of rock salt type structure is expected as the result of material-electrolyte reaction at high voltage. The forming layers are generally an additional barrier for the Li^+ ion transport and they reduce the cell performance.[41] The relative amount of interface layer to the active material is increasing as the material-electrolyte contact area increases thus it is important to know the ECSA changes during electrode operation. In some cases, the surface of the active material grains can be covered by additional protecting layer to minimize the undesired electrolyte-material interactions, or promote faster ion diffusion.[42] The coating application affects the apparent ECSA and its presence have to be considered during further calculations.

Here we present the in situ, nondestructive, electrochemical method of ECSA variations determination during material lithiation. The method is useful for the examination of a new types of electrodes, especially characterized by volume expansion/depletion such as silicon, tin, aluminum, germanium.[43]

The method relies on electrochemical impedance spectroscopy measurement (EIS) performed at arbitrarily chosen state of charge/depth of discharge (SoC/DoD) point. The correlation between a local ion concentration with a charge transfer resistance and an overpotential allows to evaluate the variations in active surface area by DC superimposed EIS measurements (DCSI-EIS).

The DCSI-EIS technique has been already introduced in the literature as a method for charge transfer (CT) changes determination. It was applied for fuel cell[44,45] as well as Li-ion electrodes.[46] However, the observed CT vs. DC profiles have been never associated with the ECSA changes. This is the first time where DCSI-EIS measurements are linked with ECSA changes via Butler-Volmer equation for in situ determination of electrochemically active surface area changes during lithiation of Li-ion electrode materials.

Experimental Section

The EIS measurements were performed by the Solartron 1260 potentiostat coupled with Solartron 1287 frequency response analyzer. Randles model equivalent circuit and data fitting were performed via zView software. The impedance data of silicon-based and graphite electrodes were fitted using a commonly used Randles model (1), whereas for LTO electrodes model (2) has been used:

(1) $R_{electrolyte} - (R_{SEI} // CPE_{SEI}) - (R_{CT} // CPE_{CT})$,

(2) $R_{electrolyte} - (R_{CT} // CPE_{CT})$;

where $R_{electrolyte}$, R_{SEI}, and R_{CT} are the electrolyte resistance, solid-electrolyte interphase (SEI) resistance, and charge transfer resistance, CPE is a constant phase element corresponding to either solid-electrolyte interphase or charge transfer and // is parallel connection.

Electrodes were prepared by a slurry deposition on a copper foil. The slurry consists of 60–80% active material, 10–25% conductive carbon, 10–15% binder dispersed in either water or N-Methyl-2-pyrrolidone (depends on a binder type – Table S1). After the slurry deposition, the electrode layer was dried in 120 °C in vacuum for 12 h. Electrodes were calendered with various pressures and a detail description of electrodes parameters are presented in Table S1.

Cells were assembled using Swagelok® 3-electrode casing. Counter electrode and reference electrode were composed of metallic lithium (Sigma Aldrich). The same electrolyte composition was used in all experiments. The electrolyte was composed of 1 M $LiPF_6$ in 3:7 fluoroethyl carbonate: ethyl methyl carbonate (FEC:EMC) + 2 w.w.% vinylidene carbonate (VC).

The N_2 adsorption/desorption experiments were conducted via the Micromeritics ASAP 2060 apparatus at 77.349 K absolute temperature in the range of 0.01 to 0.995 relative N_2 pressure $p \cdot (p^0)^{-1}$. The adsorption/desorption isotherm analysis were performed using ASAP 2060 software. The surface area was obtained using the BET method. Distribution and pore volume were calculated using the BJH method from desorption curves.

After the assembly, the cells were held for 24 h at OCV to reach an equilibrium. A full formation cycle between 0–100% DoD at 0.1 C-rate current was performed for a proper SEI formation prior actual experiment. The voltage and current flow during the following experiment are schematically shown at Figure 2. During the experiment, the cells were discharged to 0.02 V (graphite or silicon-based) or to 1.0 V (LTO) vs. reference electrode at 0.1 C-rate current (region A). During this discharge the DC current flow was stopped several times at the specified SoC levels (region B) and each time the DC-superimposed EIS measurements were performed. Before the first EIS test, the current was set to zero for 2 h to obtain the stable cell voltage and minimize the lithium concentration gradient in the electrolyte and active material grains (region B).

At the desired SoC level, the several DC-superimposed EIS (DCSI-EIS) tests were executed (region C, Figure 2c). Each individual DCSI-EIS test (region D, Figure 2d) was conducted at the different superimposed DC value starting from 0 μA and continuing for positive and negative DC values. DC absolute value increased gradually with 50 or 100 μA steps for graphite and LTO, or silicon-based electrodes, respectively. After each DCSI-EIS step the cells were resting at OCV for 10 minutes (region E, Figure 2e.) and the next experiment with opposite DC current flow direction was performed. A sequential switching of DC current direction in the following tests reduced the SoC changes during one group of DCSI-EIS experiments. We approximate the cell SoC as the set (initial) SoC in all calculation, even though the actual value slightly oscillated around mean value due to superimposed DC current flow. The SoC oscillation was less than 1% due to short time of measurement. Each DC-superimposed EIS test was executed at the selected SoC value between 100 kHz and 5–10 Hz with 30–90 μA AC amplitude (dependent on DC current value). Various active materials were researched: silicon nanopowder calendered at low (Si-nano L) and high (Si-nano H) pressure, silicon/graphite composite (Si/C), graphite (graphite) and lithium titanium oxide (LTO). Their labels and important experiment parameters are listed in Table S2.

2. Results and Discussion

2.1. Theory

After immersing the reversible electrode into the solution, the two opposite: oxidation and reduction reactions are constantly proceeding at its surface. After a short period of time the net effect of these reactions goes to zero, but the current related to both is constantly flowing through the electrode. This current is called exchange current (I_0), and its density (j_0) is very important electrochemical parameter describing the electrode tendency to undergo electrochemical reactions. The exchange current density can be treated as idle current. Applying the overpotential (η) leads to small misbalance in the ratio of oxidation to reduction current. If the j_0 absolute value is high, the misbalance related to the used overpotential will lead to high net current flow through the system even at low η.

The relation between overpotential and current density (j) is described by the Butler-Volmer equation [Eq. (2)]:

$$j = j_0\left[e^{\left(\frac{-\alpha zF}{RT}\eta\right)} - e^{\left(\frac{(1-\alpha)zF}{RT}\eta\right)}\right] \quad (2)$$

where: R, F, T, and z are gas constant, Faraday's constant, temperature, and charge number respectively, α is the empirical reaction symmetry factor characteristic for the individual electrode/electrolyte system.

At low overpotentials, Equation (2) can be simplified, since for small x, the e^x can be approximate by $(1+x)$ expression. At this small η the Butler-Volmer equation predicts the linear current-overpotential dependence according to Equation (3):

Table 1. The list of symbols, their description and units, commonly used in the text.

Symbol	Description	Units
R, T, F, z	Gas constant, temperature, Faraday constant, electron number for elemental reaction	$J \cdot mol^{-1} K^{-1}$, K, $C mol^{-1}$, dimensionless
$R_{electrolyte}$, R_{SEI}, R_{CT}	Resistance of electrolyte, resistance of SEI layer, resistance of charge transfer (all variables refer to total values for specific system)	Ω
j	Current density (function of ECSA)	$A m^{-2}$
j_0	Exchange current density	$A m^{-2}$
I	Total current flowing through external circuit	A
I_0	Total exchange current (function of ECSA)	A
$(I_0)_{eff}$	Effective exchange current affected by local surface concentration of reactive spices (function of ECSA)	A
I_{DC}	DC current applied to the system	A
η	Overpotential (total value for specific system)	V
A	Electrode electrochemically active surface area (ECSA)	m^2
C_x	Bulk concentration of indexed form of electroactive compound	$mol\,dm^{-3}$
$C_x(0)$	Surface concentration of indexed form of electroactive compound	$mol\,dm^{-3}$
N	Normalization factor (contain all variables unrelated to A, I, η	dimensionless
L	ECSA relative change	dimensionless

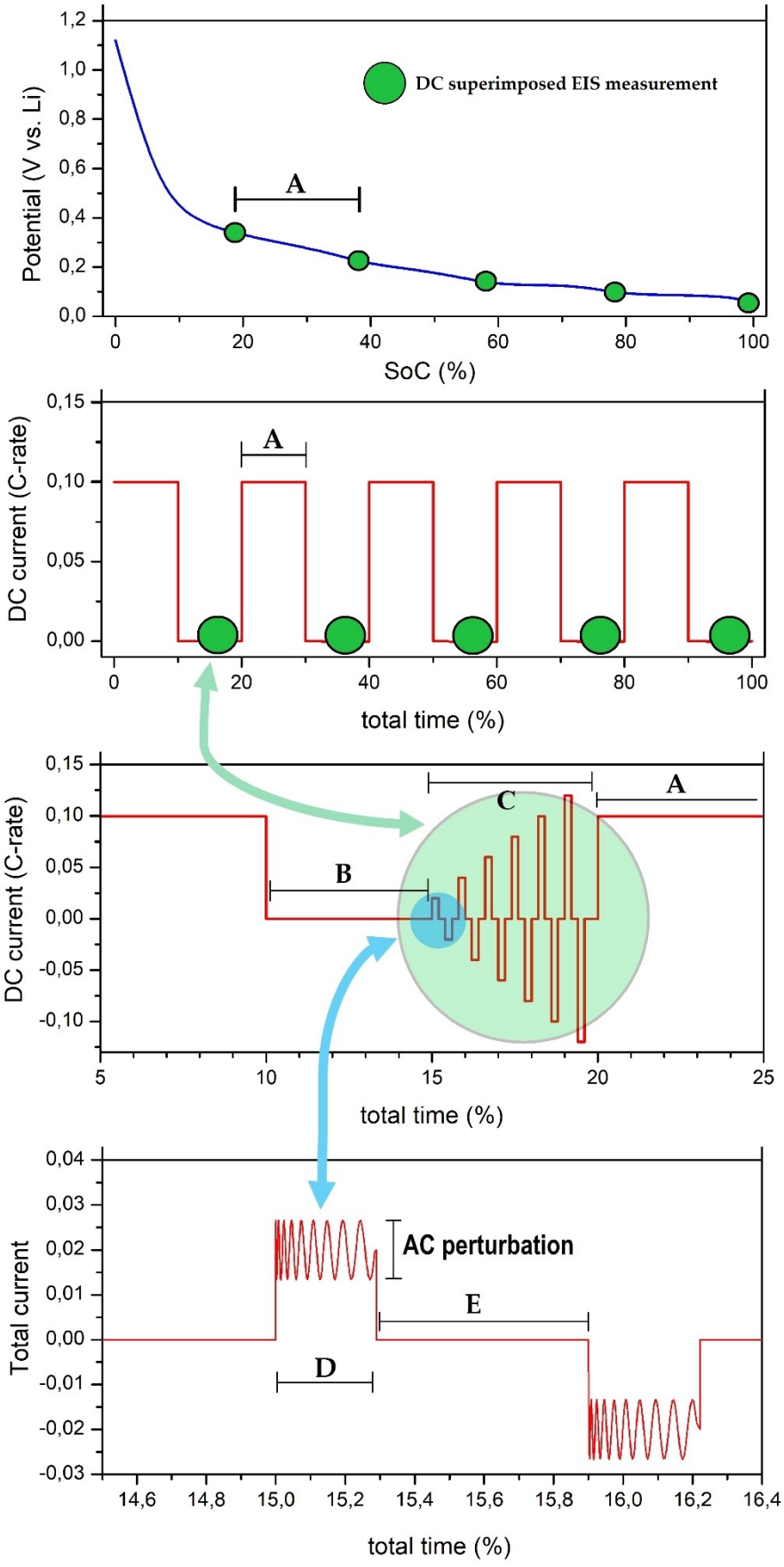

Figure 2. Schematic representation of voltage and current changes during the performed experiments.

$$j = j_0 \frac{zF}{RT}\eta \tag{3}$$

At this range the constant ratio of η/j is called charge-transfer resistance (CT or R_{CT}) given by:

$$R_{CT} = \frac{RT}{zFj_0A} \tag{4}$$

where A is an electrode area (ECSA).

The total current flowing through the electrode during the reversible faradaic reaction is limited by several resistance factors affecting a system performance. These resistances originate from kinetic restrictions: electrode material electric resistance, electrolyte solution resistance, charge transfer (CT) resistance, resistance of reactions following the CT or mass transport restrictions: diffusion and migration resistance. Depending on system properties and current density either the kinetic or mass transport resistances are limiting the cell performance. In case of Li-ion electrodes, the CT resistance is often one of the major limiting factors.[40,46–48]

The overpotential increasement leads to conditions, where Equation (3) is no longer valid. The current-overpotential relation is then described by exponential relation from the Butler-Volmer equation. However, the current related to one of the opposing reactions (either reduction or oxidation) can be neglected since the high overpotential is applied. The Butler-Volmer relation can be then described by the Tafel equation. During a further continuous overpotential increasement, the reaction is no longer kinetically restricted. The mass transport (diffusion, migration or convection) resistances start to dominate over a total system resistance and the all above equations are no longer valid.

The relation of the electrochemical process at the Li-ion electrode surface (quantified by R_{CT} value) with the Butler-Volmer equation is commonly known in the literature.[49,50] The electron transfer reaction at the electrode-electrolyte interphase is represented by Equation (1) or (2) depending on the current density.

The conditions in the DCSI-EIS experiment are quite different compared to the standard AC impedance measurement which is performed at the steady electrode conditions. The role of DC current (I_{DC}) in the DCSI-EIS experiment is to set the surface concentration gradient of the electroactive substance in the active material grains. In general, this concentration differs from the equilibrium value, so the concentration gradient and diffusion layer and formed during the experimental procedure. The I_{DC} and the effective j_{DC} ($j_{DC} = I_{DC}/A$, where A is electrochemically active surface area (ECSA)) are constant in the single experiment. After some time, the diffusion layer becomes thicker than the AC perturbation effective range which is limited due to the relatively high frequency. The shifted surface concentration appears like bulk concentration for the AC wave.

At the steady conditions the exchange current as well as R_{CT} are the internal, constant system parameters. At this state, the I_0 can be described by the Equation (5), where k^0 – standard heterogeneous rate constant, A is equal to ECSA.

$$\log I_0 = \log FAk^0 + (1-\alpha)\log C_O^* + (\alpha)\log C_R^* \tag{5}$$

The equation relates to Nernst equation via the bulk concentration of electroactive spices (C_O* and C_R*).

Normally, the R_{CT} and I_0 are connected by Equation (4). We treat the exchange current as a system property defined by the bulk concentration of reactive spices (C_O* and C_R*). In the DCSI-EIS, a surface concentration (in the active material grains) is not in equilibrium and is affected by DC current flow, however for AC wave the surface concentration acts as the bulk concentration. We can then recognize an effective exchange current for the AC perturbation at the electrode surface, at given time (t) by Equation (6):

$$(I_0)_{eff} = FAk^0[C_O(0,t)]^{(1-\alpha)}[C_R(0,t)]^{\alpha} \tag{6}$$

or through a further transformation provided in Equation (7), where $\xi = \sqrt{D_O/D_R}$ and $a = \frac{zF}{RT}\eta$:

$$(I_0)_{eff} = FAk^0 C_O^* \xi^{\alpha}\left(\frac{e^{a(1-\alpha)}}{1+e^a}\right) \tag{7}$$

The DC current affects the effective exchange current and R_{CT} by altering the surface concentration. The charge transfer resistance is inversely proportional to $(I_0)_{eff}$ according to Equation (8). The presented argument are consistent with the findings of other authors.[51,49]

$$R_{CT} = \frac{RT}{zF(I_0)_{eff}} \tag{8}$$

If DC current changes the surface concentration of electroactive species at the electrode material depth (thickness) greater than the AC perturbation effective range, the CT resistance will change accordingly to the surface concentration variation.

The absolute changes (increase or decrease due to a different current direction) of the surface electroactive species concentration due to DC current will be different for a various electrode ECSA value. At given $I_{DC,}$ the high absolute ECSA value will result in very low concentration changes because the effective current density (j_{DC}) will be low. Opposite, the low ECSA will result in a high current density and a large concentration gradient formation. Consequently, respective R_{CT} changes can be observed by DCSI-EIS experiment. The analysis of R_{CT} at different I_{DC} will then provide information about the ECSA.

The absolute value of R_{CT} in Li-ion electrode is affected by several factors including the electrode state of charge (SoC), the composition of the electrode and electrolyte, the temperature[49] and the absolute value of ECSA. The same factors influence the absolute value of $(I_0)_{eff}$. Since the DCSI-EIS is performed in the constant temperature and electrolyte composition, these factors can be neglected. At every SoC,

several individual measurements are performed with different DC current values. Since all individual measurements are done at a single and approximately stable SoC, we can neglect the effect of this parameter either.

The only parameter that affects R_{CT} changes within DCSI-EIS measurement is the ECSA. Unfortunately both $(I_0)_{eff}$ and R_{CT} are related with ECSA by Equations (4) and (6) respectively. For that reason, a direct determination of the ECSA absolute value by DCSI-EIS is impossible. However, the relative changes can be easily determined from an analysis of R_{CT} vs. I_{DC} curves.

The amplitude of AC perturbation generated during EIS experiment is generally low. Accordingly, the Butler-Volmer equation [Eq. (2)] can be used for the analysis of R_{CT} vs. I_{DC} curves. In the equation, a current density is used instead of the absolute current value. Generally, the BV equation should be applied to the system with fast mass transport and zero concentration gradient, but when the concentration gradient is present, but it is not the source of mass transfer related limitations, the similar current-overpotential relation [Eq. (9)] can be used.

$$I = I_0\left[\frac{C_o(0,t)}{C_o{}^*}e\left(\frac{-\alpha zF}{RT}\eta\right) - \frac{C_R(0,t)}{C_R{}^*}e\left(\frac{(1-\alpha)zF}{RT}\eta\right)\right] \quad (9)$$

Since it is impossible to determine the absolute value of ECSA, one has no information about the current density. To overcome this problem we introduce the "ECSA relative change" parameter – *L*, to the standard Butler-Volmer relation [Eq. (10)]:

$$I_{DC} = Nj_0(A' \bullet L)[e^{\left(\frac{-\alpha zF}{RT}\eta\right)} - e^{\left(\frac{(1-\alpha)zF}{RT}\eta\right)}] \quad (10)$$

The approximate value of j_0 and A' (ECSA) present in the equation can be determined by separate EIS measurement at $I_{DC}=0$ or by theoretical equation *(1)*. The area value obtained from Equation (1) was used as an initial value of active surface during the active surface changes calculations. Since our method determines the changes (not the absolute value), the precise initial value can be ignored. The applied initial value should however present a correct order of magnitude. The relative ECSA changes (*L*) determined by fitting the experimental results by Equation (10) has to be further normalized since the j_0 and "A'" values were just roughly estimated leading to initial "*L*" value different than 1. The normalization is done by introducing normalization factor-*N*, which generally contains all constant elements that are not dependent on I_{DC} and all correction factors related to uncertainty of j_0 and the initial surface area determination.

The I_{DC} and R_{CT} are both depend on the ECSA. The absolute value of R_{CT} can differs for different SoC levels of the same electrode, however it was not used for the calculations due to the direct relation of two mentioned parameters with ECSA. Only the R_{CT} changes with respect to I_{DC} were analyzed. Then I_{DC} is applied some surface concentration gradient is formed. The gradient amplitude is affected by two factors: ECSA and I_{DC}. The external current value is known, so at the same current flow, the largest gradient is formed when ECSA is lower. The R_{CT} is also affected by two factors: ECSA and electrode/electrolyte chemistry. The ECSA is changing through the SoC change, but the single measurement point was obtained at constant SoC (SoC change $<1\,\%$), so the ECSA was considered constant. The only thing that changed is the chemistry - concentration gradient affected by I_{DC}. So, if the gradient changes, the R_{CT} will also change. If we set the experiment at particular SoC we can assume that, if the R_{CT} change rate with respect to I_{DC} is different that it was at another SoC value, the ECSA must have been changed during SoC change.

2.2. Experimental Evaluation

In the presented research we evaluated the ECSA changes determination procedure for five different materials. Electrodes prepared from three of them contained mainly silicon or silicon-based materials: silicon nanoparticles calendered at low (Si-nano L) and high (Si-nano H) pressures and silicon/graphite composite (Si/C). Silicon is known of the high volume (and in consequence surface) change material during lithiation. We expected a very high electroactive surface change for Si-based electrodes. In addition, we examined graphite (graphite) and lithium titanium oxide (LTO) based electrodes which volume and surface change are much smaller during lithium uptake. A graphite volume change is up to 14% at full lithiation (LiC_6), mainly due to an increase in a graphene interlayer distance from 0.34 up to 0.37 nm.[21] Graphite lithiation occurs at the similar potential range as for silicon-based materials. In a consequence, the SEI passivation layer is formed at both materials (electrodes). The comparison between silicon and graphite electrodes should prove a link between observed electrochemical parameters and electrochemically active surface area changes. The amplitude of active surface area changes during lithiation is the principal difference between those materials (regardless of a different lithiation mechanism). The LTO electrode was examined to exclude the effect of the SEI layer on the observed electrochemical parameter changes. The operation potential of LTO is placed above 1.0 V, typically close to 1.5 V.[27] The SEI formation occurs mainly below 0.7 V due to an organic carbonates reduction.[52,53] The volume change during LTO lithiation is neglectable – close to 1%. Such small crystal unit volume change should result in almost zero active surface area change during lithium uptake.[54]

Silicon electrodes were calendered with different pressure to investigate the effect of this parameter on active surface area changes during lithiation. According to our assumptions (showed schematically at Figure 1), high calendering pressure should result in a low porosity and a low active surface area electrode due to an electrolyte inaccessibility into grains surface. An extremely low porosity electrode initial surface area might be approximate with its geometric surface area. After the silicon lithiation, its specific volume increases and might result in the electrode structure loosening and the great increase of the active surface area. The opposite effects are predicted for the high porosity electrodes (low calendering pressure). The high porosity results in the higher initial absolute value of ECSA

and provides a space for the silicon expansion during lithiation. As an effect, the relative surface change might be smaller compared to highly calendered electrodes. The important electrochemical and mechanical properties of examined electrodes are listed in Table S1.

The selected EIS spectra (Nyquist plots) of examined electrodes recorded at various SoC are presented at Figure S1. To determine the accuracy of the data fitting we analyzed the Nyquist plots, the phase angle vs. frequency plots and performed the Kramers–Kronig (KK) residual test. Fitting results based on previously presented Randles models are showed in Figure S2. Results of the KK tests are presented in Figure S3. A lithium ion diffusion through the SEI layer and its electrochemical reaction (CT reaction) at the electrode surface can be characterized by a very similar time constant. The silicon-based and graphite-based electrode's Nyquist plots possess a collective, overlapped semicircle related to the SEI layer resistance and capacitance, and the CT resistance and the double layer capacitance due to a similar time constant of those processes. Despite of the SoC level or the electrode material, the end of the semicircle (related to sum of electrolyte, CT and SEI resistances) tends toward a lower real impedance (Z') value as the superimposed DC current increases. The observed electrochemical response is in a good agreement with the previously stated theoretical explanation.

The LTO electrode presented very similar response indicating that CT resistance changes are responsible for the overlapped semicircle end drifting. LTO electrodes were almost free of the SEI layer, so the CT change was the only factor affecting the observed EIS plots changes. The SEI resistances determined for silicon-based and graphite electrodes were independent of I_{DC} in all cases and thus may be incorporated into the factor "N" and excluded for further calculations.

The obtained EIS spectra were used to determine charge transfer (CT) resistances vs. DC current at different SoC levels of all the investigated electrodes. Figure 3 presents the R_{CT} vs. DC current dependence in the function of SoC for the electrodes characterized by the highest (Si-nano H) and the lowest (LTO) variation of ESCA. The results for graphite, Si-nano L and Si/C composite electrodes are presented in Figure S4. The resulted dependency presents the Gaussian shape. The silicon-based electrodes reveal a different electrochemical response compared to LTO and GSM samples. The silicon electrode Gaussian curve shape is affected by SoC. The fitting curve shapes for GSM and LTO samples are independent of SoC. For those samples only "y" axis curve transition is observed during the SoC change. In general, the larger the change of the R_{CT} vs. I_{DC} shape at different SoC, the bigger the ECSA change of examined electrode is. The curve shape change determines the ECSA changes, while a simple transition of the curve along R_{CT} axis has no reflection in ECSA changes.

In the theoretical section it has been shown that the recorded absolute value of $CT_{(DC=0)}$ resistance is affected by several factors such as: the exchange current density, the symmetry factor, the local lithium ion concentration in the solution, the lithium concentration inside of the grains, and of course the ECSA value. The effect of these factors are clearly visible as the $CT_{(DC=0)}$ resistance variation during the electrode lithiation. There is no general trend in these changes because they origin from the collective effect of different factors fluctuations. The absolute value of CT is not necessary for further calculations due to the fact, that relative surface changes will be evaluated. To perform the calculations it has been assumed, that all factors affecting the CT value are constant during the single DCSI-EIS experiment (region D at Figure 2). The SoC change during the single experiment was typically less than 1% leading to the conclusion, that the exchange current density, bulk lithium concentration inside of the grains, symmetry factor, and ECSA remain constant during this short period of time. As a result, the only factor responsible for the observed different $CT_{(DC\neq0)}$ behavior was a local ion concentration close to the grain surface [Eq. (6)]. This local lithium concentration gradient is affected by the DC current density, which is directly related to the ECSA.

The resulted nonlinear (Gaussian) dependences were fitted with the modified Butler-Volmer equation [Eq. (10)]. Figure S5 shows how the normalized parameter "L" (directly reflecting the ESCA variations during lithiation) affect the accuracy of

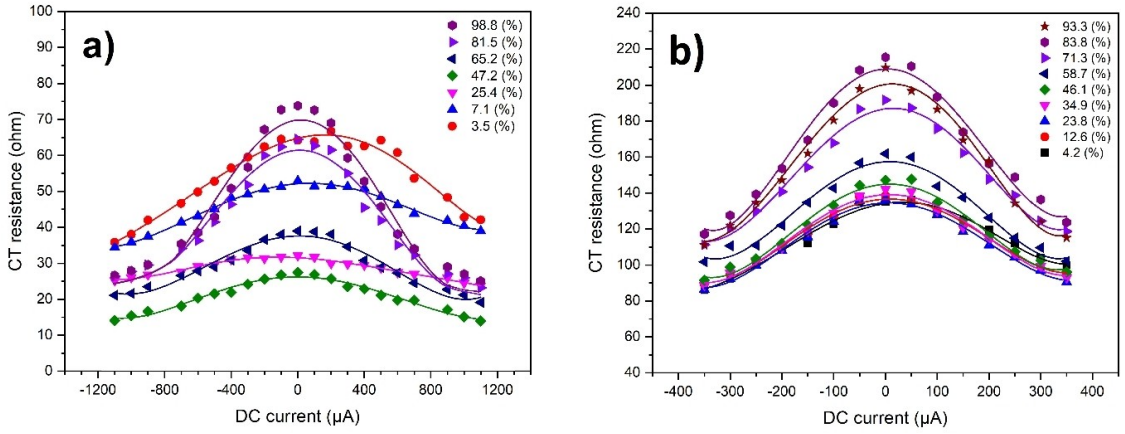

Figure 3. Charge transfer resistance vs. superimposed DC current at different SoC for (A) Si-nano(H), (B) LTO.

fitting the results with the Butler-Volmer equation. The fitted data sets were adjusted by the least squares method. The obtained and normalized parameter "L" represents the relative ECSA changes during electrode lithiation.

Recently new ways of describing the Li-ion electrode kinetics were investigated since the Volmer-Butler equation failed to predict the experiments results for very high C-rate, or during the analysis of poor electronic conductors, e.g., $LiFePO_4$.[55] The MHC (Marcus-Hush-Chidsey) model in very good agreement with the data at whole overpotential range suggesting good correlation with the true reaction mechanism. In our experiment, the applied current was clearly in the range of good BV agreement. The BV relation is a very simplified model, it misses some of the processes that can be crucial during high overpotential or C-rate application, but was proven to be a good starting point of modeling the reaction kinetics in multiple systems including LIB. We observed an increased incompatibility of BV relation with the experimental data (e.g., at $I_{DC} > 1000$ μA for Si-based electrodes), but the use of such high current was not necessary for our calculation and was excluded from ECSA determination. The main reason for BV equation fail during high current flow was probably related to uneven current distribution along the thickness of the porous electrode.

The obtained results (Figure 4) confirmed a high ECSA change during lithiation of all examined silicon-based electrodes. The highest variations were observed for strongly calendered electrode - Si-nano(H). The ECSA change exceeded 105%. Based on the available data of Si specific volume changes (c.a. 300%), the theoretical, maximal surface expansion of silicon spherical particle during lithiation is c.a. 108%. The DCSI-EIS result obtained for heavily calendered silicon electrodes reflects that theoretical maximum surface expansion. Since the Si-nano(H) sample is a real system, where Si particles are closely connected between each other due to the applied pressure, the theoretical surface expansion of the single silicon spherical particle cannot be the only reason of ECSA changes. As we expected, the ECSA of pristine, highly calendered electrode is low, due to interconnection of particles and thus an inaccessibility of the electrolyte between grains located further from the electrode surface (Figure 1). After the silicon expansion, the electrode structure becomes loose and promotes the electrolyte access to most of the grains. The relative ECSA change during this process might be close or even exceed the theoretical maximum calculated for a single particle because of addition expansion effects in the real electrode as explained above.

Weakly calendered electrodes – Si-nano(L) demonstrates a much lower ECSA changes during lithiation (up to 62%). A good initial electrolyte access to the inner grains resulted in the high initial absolute ECSA value. As the result, the observed ECSA changes were attributed mostly to the individual Si grains expansion rather than electrode macro-structure changes. The difference observed between these two electrode examples can be used for the best calendering parameter estimation or the comparison between different active materials. Generally, high ECSA variations leads to electrode structure degradation and electrolyte loss due to additional SEI layer formation.

Similar finding has been established for Si-graphite composite electrode (Si/C composite). The ECSA increased by 31% at almost 90% lithiation. Unfortunately, the experiment was not conducted at the higher lithiation level. A high mass loading of investigated electrode greatly increased the reaction overpotential leading to lithium plating during the high negative DC current flow leading to unpredictable R_{CT} vs I_{DC} changes and model failure. The data obtained during the test resulted with Li plating was then excluded from ECSA changes determination. The Si/C composite ECSA changes are very similar to

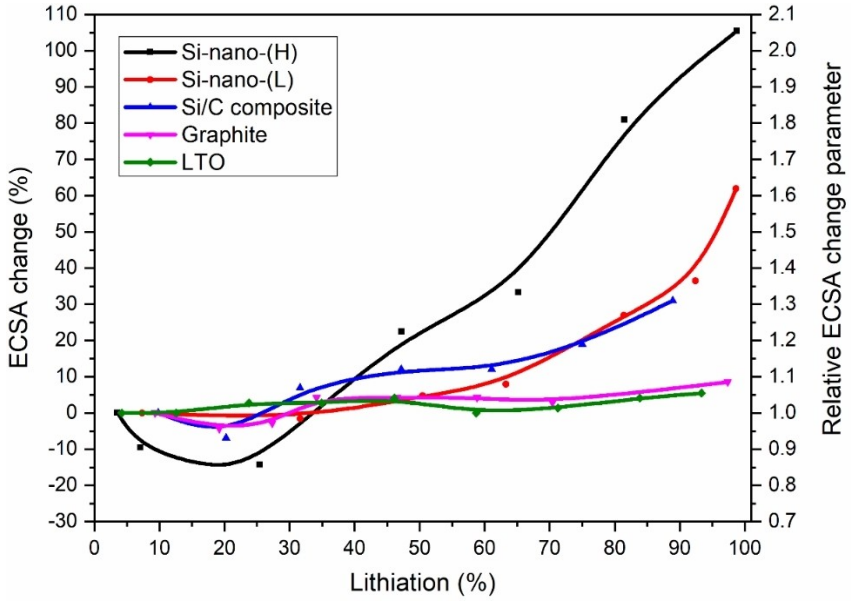

Figure 4. Determined ECSA changes during lithiation of examined electrodes.

observed for Si-nano(L) electrodes. The main difference is a more linear ECSA behavior during the composite lithiation. According to previous findings published by Berhaut et al.,[56] the Si/C composite electrodes are characterized by a number of the large macro-pores inside of the electrode structure. The very loose and elastic internal structure of this electrode allowed for the unrestrained silicon expansion leading to the linear ECSA increase during lithiation. The structure of Si-nano (L) was denser and more compact. As an effect, at the beginning of lithiation (up to 30% SoC) the ECSA remains almost constant due to the opposed effect of the silicon grain expansion and the mutual electrolyte access restrictions. The net effect of those factors was close to zero. After the certain point of SoC the silicon expansion leads to high tension generation inside the electrode structure. If the tension is greater than structure stiffness, the electrode structure starts to expand and the ECSA increases. For Si/C composite the electrode structure stiffness was low enough to enable almost unrestricted silicon expansion since the beginning of lithiation.

The graphite and LTO electrodes presented very low surface area changes during lithiation. The collective results of these electrodes confirmed that the SEI layer presence does not affect the procedure. No major difference between GSM and LTO samples led us to the conclusion that the SEI layer on the graphite electrode surface has very limited or zero impact on the performed measurements. The SEI resistance may vary at different SoC, but it can be neglected in case of the relative ECSA determination.

The obtained results are in good agreement with theoretical estimations and with our simple model of ECSA changes which is based on the common knowledge. The method accuracy was evaluated by LTO and graphite sample ECSA changes, since the silicon-based electrodes ECSA change after lithiation is hard to predict. The graphite ECSA variation is in a very good agreement with expectations. The theoretical graphite specific volume change during lithiation is close to 14%. This should theoretically lead to 6% grain surface increase during lithiation. Our results showed maximum of 8.5% increase in this electrode ECSA. The difference may be related to a minor electrode structure distention due to a graphite swelling and/or PVDF binder soaking with the electrolyte. The PVDF had showed large soaking capabilities,[57] which may lead to a slight electrode structure expansion.

The LTO electrode presented higher ECSA change than expected based on the XRD cell unit expansion data. The maximum ECSA change was up to 5.5%. PVDF soaking may be the reason of the small result deviation as stated for the graphite electrode. In case of the LTO, the presence of the very thin SEI layer is sometimes reported .[58] In our EIS Randles model we assumed no SEI on the LTO surface. This difference may be the origin of small ECSA fluctuation at the high lithiation level.

An unexpected ECSA decrease (contraction) occurred for Si-nano(H) electrode, as well as for other samples (except LTO), during the first part of the lithiation (typically SoC up to 30%). One of the reasons of such phenomena might be an induced electrolyte access blockage between expanding active material grains. The most severe ECSA contraction was observed for highly calendered silicon electrode due to a low porosity and a high stiffness of this sample. The silicon expansion led to the certain amount of grains to be trapped with no electrolyte access and thus to be eliminated from taking part in the electrochemical reaction. Over some point of the reaction progress the electrode structure was distended and the ECSA growth was observed. These findings bring a new light into the silicon-composite electrode stability. By using our new experimental technique, it is possible to determine the level of lithiation where electrode structure, matrix structure etc., starts to distend due to silicon swelling. This phenomenon can be adopted for increasing the cycle performance of Li-ion cells utilizing silicon-based active materials. The restriction of the silicon electrode SoC to the ECSA contraction region (e.g., by narrowing voltage window or by a proper mass (capacity) balance between anode and cathode) can indicate the great increase of the electrode structure stability. In the ECSA contraction window, the mechanical stability of the electrode is higher, than the internal force caused by the silicon swelling. Electrode operation in this region may result in extended cycle stability.

The data analysis proved, that our new method is capable of the ECSA variation determination regardless the nature of electrode active material. We believe that the methods can also be implemented for carbon coated materials that are frequently used in Li-ion batteries. The presented technique provides several important information about the electrode mechanical structure during lithiation leading to a better understanding of ongoing changes and possible degradation reasons. The high ECSA changes during lithiation might be responsible for the electrode structure degradation and the electrolyte loss due to the SEI formation on certain anode materials. Very high ECSA changes – close to the theoretical maximum, are the effect of the low initial porosity leading to electrolyte access restrictions into the inner electrode structure. The observation of the surface area contraction during the initial lithiation phase can differentiate the nature of the electrode matrix. The large contraction leads to a conclusion, that the electrode matrix is strong enough to maintain its structure during the active material expansion. A lack of contraction for silicon or other volume changing materials, is the result of the high initial porosity or the insufficient matrix durability. Based on those conclusions the electrode production method, e.g., calendering pressure and composition, can be easily evaluated and adjusted, guiding to the best practical cell properties. The only observed limitation of this method was related to a possible lithium plating at a high DC current (especially for a high electrode mass loading) and a high result inconsistency at very low SoC ($<3\%$) related to large electrode potential changes in this range. Another limitation of the technique may be related with recently investigated, T-shaped graphene coating on active materials.[59] An amorphous carbon coating should have no effect on our calculations (method), because the grain surface, covered by the carbon layer, have the same electrochemical properties in every point. The "anti T-shape" graphene coating is generating two different "areas" at

the grain surface with different Li^+ diffusion properties (blocked or promoted). The SEI layer can be formed on the whole grain regardless of the local Li^+ diffusion properties leading to major error during DCSI-EIS analysis.

The ECSA changes analysis can also greatly improve the data accuracy obtained during different electrochemical measurements of volume changing materials. During all electrochemical tests the obtained raw data are directly dependent on ECSA. During the analysis of intercalation-type crystal materials, the volume change is low enough (typically less than 10%) to neglect the ECSA variations during the experiment. The high volume changes of silicon, SiO_x[60] and some other alloys or conversion-type materials, leads to a great ECSA changes that cannot be neglected. If do so, the obtained results will present large error, and will cause wrong conclusions about the material electrochemical behavior. We believe that the implementation of our in situ active surface area variation determination technique for the volume changing material research will greatly improve future experiments in the field.

3. Conclusions

The article presents a new method of in situ analysis of active surface area changes of the Li-ion negative electrodes. The connection between the local ion concentration with charge transfer resistance, and overpotential allowed for active surface changes evaluation by DC superimposed EIS measurements. The obtained charge transfer resistance vs. DC current curves can be fitted with the Butler-Volmer equation due to the relative dependence of electrochemical parameters. For the same reason other variables (except the active surface area) can be neglected leading to accurate results at the wide SoC range for different materials. The method is not affected by the SEI layer presence, the active material composition nor the lithiation mechanism (intercalation or alloy formation). The method application to positive intercalation materials should be possible since the results are independent from the material type.

In the field of Li-ion battery research, a geometric electrode area is generally used for electrochemical parameters evaluation. This approximation causes a large deviation of obtained results, especially within different laboratories due to different sample preparation conditions. The geometric surface area approximation may be enough for intercalation-type material, however new types of lithium-alloy materials need a different approach. A high volume and surface change during lithiation in those materials (silicon, tin, aluminum, germanium etc.) may results in major changes in the electrode electrochemical response. The electrochemical signal change can be easily mistaken with material property changes, while it is caused directly by the electrode active surface area change. Our new method allows for the surface area change evaluation during the material lithiation and, in consequence, leads to a proper result interpretation. In addition, the analysis of ECSA profiles provides the information about the electrode matrix structure stability and the calendering effect on the lithiation induced electrode swelling. The application of this information and a proper production parameters optimization to the full cell system containing silicon-based anode may improve the cell cycle life. We believe that our method can become a standard procedure implemented in every research focusing on volume changing active materials and their electrochemical parameters.

Acknowledgements

This project has been partially funded by the European Union's Horizon 2020 research and innovation programme, under grant agreement No. 685716 and The National Centre for Research and Development, Techmatstrateg programme, under grant agreement No. TECHMATSTRATEG1/347431/14/NCBR/2018.

Conflict of Interest

The authors declare no conflict of interest.

Keywords: Li-ion · surface area · impedance · silicon · electrode · volume change

[1] M. O. Guler, M. Guzeler, D. Nalci, M. Singil, E. Alkan, M. Dogan, A. Guler, H. Akbulut, *Appl. Surf. Sci.* **2018**, *446*, 122–130.
[2] H. Tian, F. Xin, X. Wang, W. He, W. Han, *J. Mater.* **2015**, *1*, 153–169.
[3] Z. Sun, Z. Chen, Q. Fu, X. Jiang, *IOP Conf. Ser. Mater. Sci. Eng.* **2017**, *182*, 012011.
[4] M. N. Obrovac, L. J. Krause, *J. Electrochem. Soc.* **2007**, *154*, A103–A108.
[5] C. Cao, I. I. Abate, E. Sivonxay, B. Shyam, C. Jia, B. Moritz, T. P. Devereaux, K. A. Persson, H. G. Steinrück, M. F. Toney, *Joule* **2019**, *3*, 762–781.
[6] M. Ratyński, B. Hamankiewicz, M. Krajewski, M. Boczar, A. Czerwiński, *RSC Adv.* **2018**, *8*, 22546–22551.
[7] M. Gu, Y. Li, X. Li, S. Hu, X. Zhang, W. Xu, S. Thevuthasan, D. R. Baer, J.-G. Zhang, J. Liu, C. Wang, *ACS Nano* **2012**, *6*, 8439–8447.
[8] V. A. Sethuraman, V. Srinivasan, A. F. Bower, P. R. Guduru, *J. Electrochem. Soc.* **2010**, *157*, A1253–A1261.
[9] S. Tardif, E. Pavlenko, L. Quazuguel, M. Boniface, M. Maréchal, J.-S. Micha, L. Gonon, V. Mareau, G. Gebel, P. Bayle-Guillemaud, F. Rieutord, S. Lyonnard, *ACS Nano* **2017**, *11*, 11306–11316.
[10] A. F. Bower, P. R. Guduru, V. A. Sethuraman, *J. Mech. Phys. Solids* **2011**, *59*, 804–828.
[11] R. Deshpande, Y.-T. Cheng, M. W. Verbrugge, A. Timmons, *J. Electrochem. Soc.* **2011**, *158*, A718–A724.
[12] Z. Cui, F. Gao, J. Qu, *J. Mech. Phys. Solids* **2013**, *61*, 293–310.
[13] A. B. Freidin, I. K. Korolev, S. P. Aleshchenko, E. N. Vilchevskaya, *Int. J. Fract.* **2016**, *202*, 245–259.
[14] M. Poluektov, A. Freidin, Ł. Figiel, *Modell. Simul. Mater. Sci. Eng.* **2019**, *27*, 084005.
[15] M. Lukaszewski, M. Soszko, A. Czerwiński, *Int. J. Electrochem. Sci.* **2016**, *11*, 4442–4469.
[16] S. Trasatti, O. A. Petrii, *Pure Appl. Chem.* **1991**, *63*, 711–734.
[17] G. Jarzabek, Z. Borkowska, *Electrochim. Acta* **1997**, *42*, 2915–2918.
[18] B. Lamy, C. Beden, T. N. R. De Tacconi, A. Arvia, *J. Electrochim. Acta* **1990**, 35, 691–704.
[19] E. Herrero, L. J. Buller, H. D. Abruña, *Chem. Rev.* **2001**, *101*, 1897–1930.
[20] S. Trassati, O. A. Petrii, *Pure Appl. Chem.* **1991**, *63*, 711–734.
[21] M. Ratynski, B. Hamankiewicz, M. Krajewski, M. Boczar, D. Ziolkowska, A. Czerwinski, *Carbon* **2019**, *145*, 82–89.
[22] M. Krajewski, B. Hamankiewicz, M. Michalska, M. Andrzejczuk, L. Lipinska, A. Czerwinski, *RSC Adv.* **2017**, *7*, 52151–52164.

[23] M. Ratyński, B. Hamankiewicz, A. Czerwiński, *Przem. Chem.* **2017**, *96*, 90–94.
[24] S. P. Woo, S. H. Lee, K. S. Lee, Y. S. Yoon, *Mater. Lett.* **2014**, *129*, 80–83.
[25] Y.-H. Jin, S.-H. Lee, H.-W. Shim, K. H. Ko, D.-W. Kim, *Electrochim. Acta* **2010**, *55*, 7315–7321.
[26] A. Suryawanshi, M. Biswal, D. Mhamane, P. Yadav, A. Banerjee, P. Yadav, S. Patil, V. Aravindan, S. Madhavi, S. Ogale, *Appl. Mater. Today* **2016**, *2*, 1–6.
[27] M. Krajewski, M. Michalska, B. Hamankiewicz, D. Ziolkowska, K. P. Korona, J. B. Jasinski, M. Kaminska, L. Lipinska, A. Czerwinski, *J. Power Sources* **2014**, *245*, 764–771.
[28] M. Michalska, M. Krajewski, D. Ziolkowska, B. Hamankiewicz, M. Andrzejczuk, L. Lipinska, K. P. Korona, A. Czerwinski, *Powder Technol.* **2014**, *266*, 372–377.
[29] H. Giesche, *Part. Part. Syst. Charact.* **2006**, *23*, 9–19.
[30] T. Vorauer, J. Rosc, P. H. Jouneau, B. Fuchsbichler, S. Koller, R. Brunner, *Microsc. Microanal.* **2017**, *23*, 2026–2027.
[31] R. Koerver, W. Zhang, L. De Biasi, S. Schweidler, A. O. Kondrakov, S. Kolling, T. Brezesinski, P. Hartmann, W. G. Zeier, J. Janek, *Energy Environ. Sci.* **2018**, *11*, 2142–2158.
[32] A. O. Kondrakov, A. Schmidt, J. Xu, H. Geßwein, R. Mönig, P. Hartmann, H. Sommer, T. Brezesinski, J. Janek, *J. Phys. Chem. C* **2017**, *121*, 3286–3294.
[33] W. Li, H. Y. Asl, Q. Xie, A. Manthiram, *J. Am. Chem. Soc.* **2019**, *141*, 5097–5101.
[34] K. Funayama, T. Nakamura, N. Kuwata, J. Kawamura, T. Kawada, K. Amezawa, *Electrochemistry* **2015**, *83*, 894–897.
[35] M. Ecker, T. K. D. Tran, P. Dechent, S. Käbitz, A. Warnecke, D. U. Sauer, *J. Electrochem. Soc.* **2015**, *162*, A1836–A1848.
[36] F. Ozanam, M. Rosso, *Mater. Sci. Eng. B* **2016**, *213*, 2–11.
[37] A. A. Arie, J. K. Lee, *Phys. Scr.* **2010**, T139, 14013.
[38] N. Ding, J. Xu, Y. X. Yao, G. Wegner, X. Fang, C. H. Chen, I. Lieberwirth, *Solid State Ionics* **2009**, *180*, 222–225.
[39] C. C. Nguyen, S.-W. Song, *Electrochim. Acta* **2010**, *55*, 3026–3033.
[40] M. Ratynski, B. Hamankiewicz, M. Krajewski, M. Boczar, A. D. Buchberger, A. Czerwiński, *Electrocatalysis* **2020**, *11*, 160–169.
[41] W. Zhang, D. Wang, W. Zheng, *J. Energy Chem.* **2020**, *41*, 100–106.
[42] D. Wang, W. Zhang, N. E. Drewett, X. Liu, S. J. Yoo, S. G. Lee, J. G. Kim, T. Deng, X. Zhang, X. Shi, W. Zheng, *ACS Cent. Sci.* **2018**, *4*, 81–88.
[43] H. Tian, F. Xin, X. Wang, W. He, W. Han, *J. Mater.* **2015**, *1*, 153–169.
[44] J. Zhang, Y. Tang, C. Song, Z. Xia, H. Li, H. Wang, J. Zhang, *Electrochim. Acta* **2008**, *53*, 5315–5321.
[45] Y. Tang, J. Zhang, C. Song, H. Liu, J. Zhang, H. Wang, S. MacKinnon, T. Peckham, J. Li, S. McDermid, P. Kozak, *J. Electrochem. Soc.* **2006**, *153*, 18–20.
[46] M. Itagaki, K. Honda, Y. Hoshi, I. Shitanda, *J. Electroanal. Chem.* **2015**, *737*, 78–84.
[47] M. Ratyński, B. Hamankiewicz, M. Krajewski, M. Boczar, A. Czerwiński, *RSC Adv.* **2018**, *8*, 22546–22551.
[48] V. A. Nikitina, *Curr. Opin. Electrochem.* **2020**, *19*, 71–77.
[49] M. Nakayama, H. Ikuta, Y. Uchimoto, M. Wakihara, *J. Phys. Chem. B* **2003**, *107*, 10603–10607.
[50] R. Hausbrand, W. Jaegermann, *Encyclopedia of Interfacial Chemistry*, **2018**, 232–245.
[51] A. J. Bard, L. R. Faulkner, *Electrochemical Methods Fundamentals and Applications-2nd ed.* **2001**.
[52] K. Xu, *Chem. Rev.* **2004**, *104*, 4303–4418.
[53] B. Philippe, R. Dedryvère, J. Allouche, F. Lindgren, M. Gorgoi, H. Rensmo, D. Gonbeau, K. Edström, *Chem. Mater.* **2012**, *24*, 1107–1115.
[54] M. Krajewski, B. Hamankiewicz, A. Czerwiński, *Electrochim. Acta* **2016**, *219*, 277–283.
[55] P. Bai, M. Z. Bazant, *Nat. Commun.* **2014**, *5*, 3585–3592.
[56] C. L. Berhaut, D. Z. Dominguez, P. Kumar, P.-H. Jouneau, W. Porcher, D. Aradilla, S. Tardif, S. Pouget, S. Lyonnard, *ACS Nano* **2019**.
[57] S.-Y. Lee, Y. Choi, S.-H. Kwon, J.-S. Bae, E. Duck Jeong, *J. Ind. Eng. Chem.* **2019**, *74*, 216–222.
[58] Y.-B. He, M. Liu, Z.-D. Huang, B. Zhang, Y. Yu, B. Li, F. Kang, J.-K. Kim, *J. Power Sources* **2013**, *239*, 269–276.
[59] J. Kim, T. Deng, X. Zhang, X. Shi, W. Zheng, *ACS Cent. Sci.* **2018**, *4*, 81–88.
[60] Y. Liu, J. Ruan, F. Liu, Y. Fan, P. Wang, *J. Alloys Compd.* **2019**, *802*, 704–711.

Manuscript received: April 21, 2020
Revised manuscript received: May 15, 2020
Accepted manuscript online: May 15, 2020
Version of record online: June 15, 2020